Chapter 3
Anisotropy

Cold worked and extruded materials always exhibit a measure of anisotropy, or "texture" where the mechanical properties exhibit directional properties. The rolling process used to create sheet metals orients the material grains and precipitates/inclusions in the rolling direction and thus induces anisotropy. Typically, bulk materials that exhibit texture effects are treated as orthotropic while sheet metals are commonly assumed to possess planar isotropy and normal anisotropy. To characterize the anisotropy of sheet materials, uniaxial tensile tests are performed with the samples fabricated from the material in different directions relative to the rolling direction. The R-value quantifies the measure of anisotropy and is defined as the ratio of the transverse strain to the through-thickness strain as shown in Fig. 3.1 and Eq. (3.1)

$$R = \frac{\varepsilon_w}{\varepsilon_t} \tag{3.1}$$

An isotropic material will have an R-value of unity while a higher R-value indicates that the material has a higher resistence to thinning with higher through-thickness strength. An average value of the anisotropy parameter should be computed from the weighted average of samples obtained from the material at orientations of 0°, 45° and 90° to the rolling direction as

$$R = \frac{R_0 + 2R_{45} + R_{90}}{4} \tag{3.2}$$

The R-value is generally taken as a material constant evaluated at a typical strain of 20 % in the tension test although some anisotropic yield criterion are capable of modeling a dynamic R-value that evolves with deformation.

Z. Chen and C. Butcher, *Micromechanics Modelling of Ductile Fracture*,
Solid Mechanics and Its Applications 195, DOI 10.1007/978-94-007-6098-1_3,

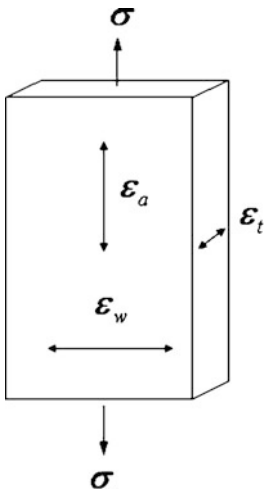

Fig. 3.1 Definition and measurement of normal anisotropy from a uniaxial tensile test

3.1 The Hill-48 Anisotropic Yield Criterion

The yield criterion of Hill (1948) has been widely used to characterize the anisotropy of sheet metals and can be considered the default or standard anisotropic model like the von Mises criterion is for isotropic materials. The Hill-48 criterion is not the ideal anisotropic yield criterion for many materials but it is a straightforward model that is readily implemented into numerical codes and well suited for analytical modeling. Additionally, the criterion requires a small number of physically-based parameters that can be directly identified from a series of tensile tests. For sheet metals where the stress state is approximately plane stress, only four parameters are required. More advanced non-quadratic anisotropic yield criterion such as the Barlat yield functions (Barlat 1987; Barlat and Lian 1989; Barlat et al. 1991, 1997; Cazacu and Barlat 2003; Cazacu et al. 2006) are widely used in industrial applications but are not well suited for analytical study due to the large number of phemenological calibration parameters and complex flow rules. The Hill-48 quadratic yield criterion for orthotropic materials can be expressed as follows

$$2\Phi(\sigma_{ij}) = F(\sigma_{22}-\sigma_{33})^2 + G(\sigma_{33}-\sigma_{11})^2 + H(\sigma_{11}-\sigma_{22})^2 + 2L\sigma_{23}^2 + 2M\sigma_{31}^2 + 2N\sigma_{12}^2 = 1 \tag{3.3}$$

where the six material constants, F, G, H, L, M, N, define the anisotropic properties of the yield surface. If the tensile yield stresses in the principal anisotropic directions are denoted as σ_0, σ_{90} and σ_t, that correspond to the rolling, transverse and thickness directions of sheet materials, the anisotropic constants are expressed as

$$\frac{1}{\sigma_0^2} = G + H \quad \frac{1}{\sigma_{90}^2} = H + F \quad \frac{1}{\sigma_t^2} = F + G$$
$$2F = \frac{1}{\sigma_{90}^2} + \frac{1}{\sigma_t^2} - \frac{1}{\sigma_0^2} \quad 2G = \frac{1}{\sigma_t^2} + \frac{1}{\sigma_0^2} - \frac{1}{\sigma_{90}^2} \quad 2H = \frac{1}{\sigma_0^2} + \frac{1}{\sigma_{90}^2} - \frac{1}{\sigma_t^2} \qquad (3.4a–f)$$

The remaining parameters can be obtained from the shear yield stresses as

$$2L = \frac{1}{\tau_0^2} \quad 2M = \frac{1}{\tau_{90}^2} \quad 2N = \frac{1}{\tau_t^2} \qquad (3.5a–c)$$

For plane stress, the yield criterion reduces to

$$2\Phi(\sigma_{ij}) = (G+H)\sigma_{11}^2 - 2H\sigma_{11}\sigma_{22} + (H+F)\sigma_{22}^2 + 2N\sigma_{12}^2 = 1 \qquad (3.6)$$

and the anisotropy coefficients can be related to the R-values using the associated flow rule to obtain

$$R_0 = \frac{H}{G} \quad R_{90} = \frac{H}{F} \quad R_{45} = \frac{N}{F+G} - \frac{1}{2} \qquad (3.7a–c)$$

The relationship between the yield stresses and R-values in the plane of the sheet can be defined as

$$\frac{\sigma_0}{\sigma_{90}} = \sqrt{\frac{R_0(1+R_{90})}{R_{90}(1+R_0)}} \qquad (3.8)$$

From Eq. (3.8), the condition for the applicability of the Hill-48 criterion is that when $R_0 > R_{90}$, $\sigma_0 > \sigma_{90}$ and this is not the case for some materials such as certain aluminum alloys. Assuming planar isotropy, $R_0 = R_{45} = R_{90} = R$, the yield criterion reduces to

$$\frac{1}{1+R}\left[\sigma_{11}^2 + \sigma_{22}^2 - R(\sigma_{11} - \sigma_{22})^2 + 2(2R+1)\sigma_{12}^2\right] - \sigma_0^2 = 0 \qquad (3.9)$$

3.2 Material Anisotropy in Porous Ductile Materials

The majority of research in developing damage-based constitutive models has focused on assuming a void with a constant shape (typically spherical or cylindrical) embedded within an incompressible isotropic matrix. In the past decade, a concerted effort has been made to account for void-induced anisotropy effects by

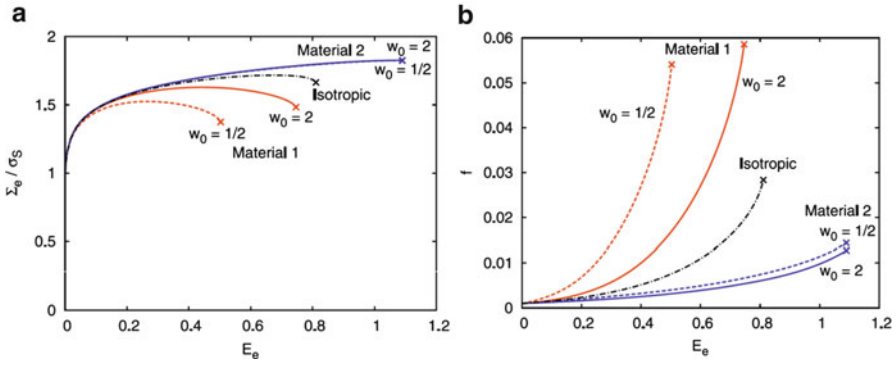

Fig. 3.2 Results of unit-cell calculations for two transversely isotropic matrix materials containing either oblate (w0 = 1/2) or prolate (w0 = 2) voids. (**a**) Normalized effective stress with the effective strain and (**b**) evolution of the void volume fraction. The initial porosity is 0.1 % with a matrix hardening exponent of 0.1 with a constant stress triaxiality ratio of unity. For comparison, the results for an initially spherical void in an isotropic matrix are shown. (Reprinted with permission from Keralavarma and Benzerga 2010. Copyright 2010 Elsevier)

relaxing the constraint that the void shape remains constant and instead modelling the void as a spheroid (ellipsoid of revolution) that evolves with deformation. It has been shown in many works that void shape-induced anisotropy can have a considerable influence on the material response (Budiansky et al. 1981; Gologanu et al. 1997; Kailasam and Ponte Castenada 1998; Pardoen and Hutchinson 2000; Aravas and Ponte Casteneda 2004; Danas and Ponte Casteneda 2009). However, relatively few studies have addressed the issue of anisotropic behaviour of the matrix material. Liao et al. (1997) extended Gurson's (1977) model for cylindrical voids to account for anisotropy in an approximate manner that is suitable for materials with normal anisotropy. Similar extensions were performed by Chein et al. (2001) and Wang and Pan (2004). The assumption of a constant spherical void in these anisotropic models is justified since considering void shape evolution significantly increases the complexity of the model because the void orientation vectors must be considered along with the directions of anisotropy. The influence of mechanical anisotropy on the response of a porous material is presented in Fig. 3.2.

Benzerga and Besson (2001) first accounted for the influence of both void shape and orthotropy and recently Moncheit et al. (2008) performed a limit analysis to obtain an analytical solution for a matrix material with elliptical voids that obeys the Hill (1948) model for anisotropy. A few attempts have been made in this area in recent years through the continual development of advanced anisotropic damage-based yield criteria that also account for anisotropy effects due to void shape (Benzerga et al. 2004) and orientation (Danas and Aravas 2012; Keralavarma and Benzerga 2010).

The lack of attention to material anisotropy in the development of damage-based material models can perhaps be attributed to the inherent difficulty in developing a general anisotropic model. Researchers in this area rely upon unit cell simulations

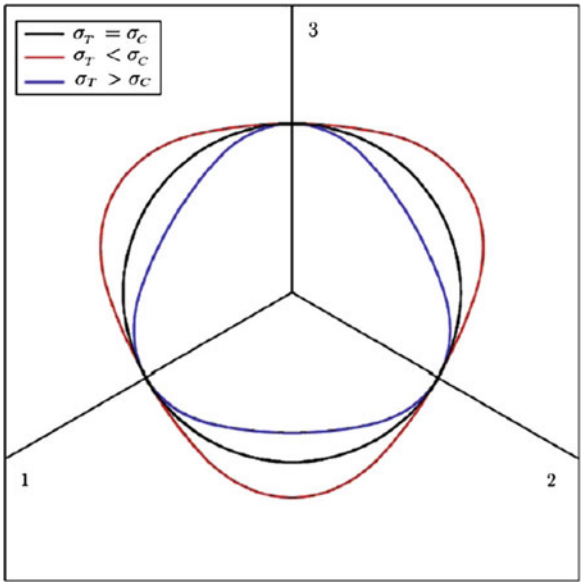

Fig. 3.3 Representation of the octahedric plane of Cazacu et al.'s (2006) isotropic yield surface corresponding to a ratio between the yield stress in tension and compression: $\sigma_T/\sigma_c = 0.82$, $\sigma_T/\sigma_c = 1$ (von Mises) and $\sigma_T/\sigma_c = 1.21$ (Reprinted with permission from Cazacu and Stewart 2009. Copyright 2006 Elsevier)

to model void growth, shape evolution and coalescence under a variety of stress states and use this data to develop their constitutive models. From a practical perspective, the assumption of an isotropic matrix enables the results of these studies to be readily generalized to the whole range of isotropic materials through the matrix hardening exponent. Conversely, anisotropy cannot be characterized in such a general manner as the anisotropy coefficients are specific to the material of interest and the yield criterion used to describe the matrix. The choice of the appropriate yield criterion is related to the material crystal structure (FCC, BCC, HCP) and may use non-quadratic yield surfaces that contain many calibration parameters that are determined from a variety of experiments. As a result, it is difficult to generalize unit cell results for void growth and shape evolution to another material. This problem becomes particularly acute when considering materials with an HCP crystal structure.

Fortunately, there has been a renewed interest in accounting for anisotropy effects on ductile fracture as industry has moved to using lighter weight, higher strength components out of more exotic and advanced aluminum and magnesium alloys that display significant anisotropy and damage sensitivity. The aforementioned anisotropic models are suitable for materials with cubic crystal structures such as most steels and aluminums because they assume the same yield stress in both tension and compression. For magnesium and titatium alloys that possess an HCP crystal structure, a tension-compression asymmetry in yielding is observed because the deformation mechanisms are related to twinning in compression and non-Schmid slip in tension (Cazacu and Stewart 2009). The variation of an undamaged yield surface with varying degrees of tension-compression asymmetry is shown in Fig. 3.3.

Magnesium alloys are of great interest in particular to the automotive industry as they offer significant weight reduction and gains in fuel efficiency, but are notoriously anisotropic and prone to void-induced cracking. Cazacu and Stewart (2009), Yoon et al. (2011) and Stewart and Cazacu (2011) have made progress in modelling void damage in HCP materials by extending the Gurson (1977) model for spherical voids into the Barlat-type yield criterion of Cazacu et al. (2006). It should be noted that unlike the traditional Gurson-based models that predict no void growth or material softening in shear-dominated stress states, the HCP damage models contain an explicit dependence upon the third invariant of the stress deviator due to their tension-compression asymmetry.

The proceeding sections will review the unit cell concept and its application to a porous sheet metal to first establish a lower bound solution for an isotropic, rigid-plastic matrix. In the sequel, the matrix material is considered as anisotropic and a quasi-exact yield criterion will be developed using fundamental unit cell theory. Finally, the models will be compared with existing models in the literature and with experimental results for the yielding of porous materials.

3.3 An Approximate Unit Cell for Porous Sheet Metals

Following the approach of Gurson (1977), the microstructure of the porous material is idealized as a periodic distribution of cylindrical unit cells with an interior cylindrical void. For sheet metals, the geometry can be reduced from a cylinder to a disk from the assumption of plane stress and subjecting the cell to a general biaxial loading that mimics a sheet metal forming operation as shown in Fig. 3.4.

The isolated unit cell is best analyzed using a polar coordinate system, $r-\theta$, as shown in Fig. 3.4b. The cell model has an outer radius, b, an inner radius, a, and an infinitesimial thickness, t. The porosity of the unit cell is thus defined as

$$f = \frac{a^2}{b^2} \tag{3.10}$$

3.3.1 Stress and Strain Rate Fields Inside the Unit Cell

From an analytical perspective, the two extreme conditions for the stress field within the unit cell are either: completely elastic or completely plastic. In reality, the stress fields will lie between these two cases where plastic deformation occurs in the vicinity of the void with the remaining material in an elastic state. This situation can be classified as “partially plastic with rigid sections”. The influence of the void distorts the stress and strain fields within the unit cell at distances up to ten times the

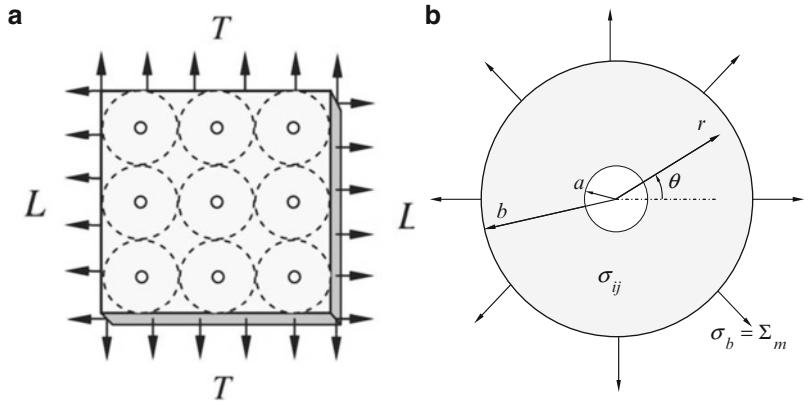

Fig. 3.4 (**a**) Idealized periodic microstructure of a porous sheet material (*left*) and (**b**) single unit cell approximated as a disc due to the assumption of plane stress (infinitesimal sheet thickness). The isolated unit cell experiences uniform radial stresses on its surface and the voids are assumed to remain cylindrical while subjected to in-plane tractions in the longitudinal direction, L, and transverse direction, T (Reprinted with permission from Landry and Chen (2011). Copyright: Elsevier)

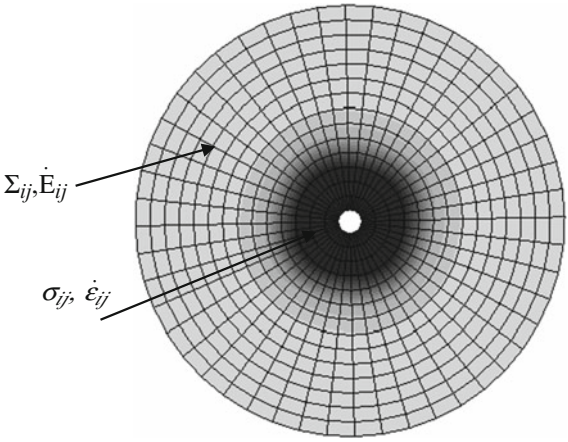

Fig. 3.5 Finite-element description of the distortional effect of the void on the stress field. The *darkest area* neighbouring the void indicates the high stress level in the vicinity of the void and describes the microscopic stresses. The remaining region of the unit cell describes the uniform macroscopic stress distribution. The influence of the void on the strain distribution is similar

void radius and the stress concentration effect of the void is illustrated in Fig. 3.5. The analytical description of the two extreme stress conditions in the unit cell will be discussed in the subsequent sections.

3.3.2 Elastic Stress State in the Unit Cell

Since the stresses and strains are linearly related in the elastic regime, the principle of superposition can be used to obtain the resultant stress or strain in a system from the algebraic sum of their effects (Bayoumi 1999). The principle of superposition

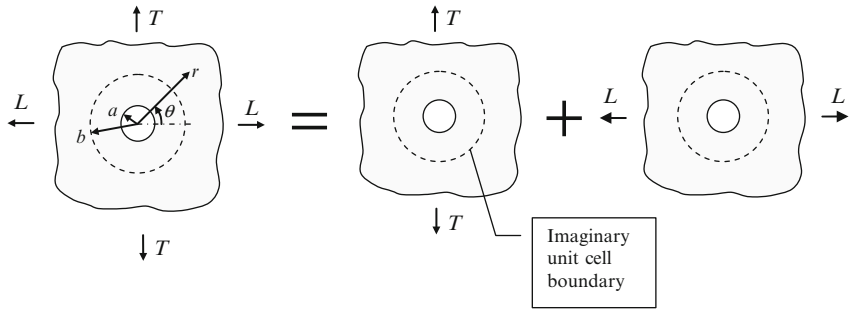

Fig. 3.6 Schematic representation of the linear decomposition of a biaxial stress state into a series of separate, isolated loadings using the principle of superposition

can be invoked to decompose the general biaxial loading on the unit cell into two separate uniaxial loading conditions as demonstrated in Fig. 3.6.

By applying the governing stress equations, biharmonic equations and equilibrium equations, we can obtain a solution for the microscopic stress fields as

$$\sigma_r^L = \frac{L}{2}\left[\left(1-x^{-2}\right)+\left(1-4x^{-2}+3x^{-4}\right)\cos(2\theta)\right] \quad x = r/a$$
$$\sigma_\theta^L = \frac{L}{2}\left[\left(1+x^{-2}\right)-\left(1+3x^{-4}\right)\cos(2\theta)\right]$$
$$\sigma_{r\theta}^L = -\frac{L}{2}\left[1+2x^{-2}-3x^{-4}\right]\sin(2\theta) \qquad (3.11\text{–}3.13)$$

where σ_{ij}^L is the microscopic stress field due to the loading, L, and x is the normalized radial distance away from the void with $x = 1$ corresponding to the surface of the void. Similarly, the stress solutions for the transverse uniaxial case, σ_{ij}^T, are readily obtained by subtracting an angle of $\pi/2$ in Eqs. (3.11–3.13). The complete solution for the elastic microscopic stress fields is

$$\sigma_{ij} = \sigma_{ij}^L + \sigma_{ij}^T$$
$$\sigma_{r\theta} = -\frac{L}{2}\left(1+2x^{-2}-3x^{-4}\right)\sin(2\theta) + -\frac{T}{2}\left(1+2x^{-2}-3x^{-4}\right)\sin(2\theta-\pi)$$
$$\sigma_{\theta\theta} = \frac{L}{2}\left[\left(1+x^{-2}\right)-\left(1+3x^{-4}\right)\cos(2\theta)\right]+\frac{T}{2}\left[\left(1+x^{-2}\right)-\left(1+3x^{-4}\right)\cos(2\theta-\pi)\right]$$
$$\sigma_{rr} = \frac{L}{2}\left[\left(1-x^{-2}\right)+\left(1-4x^{-2}+3x^{-4}\right)\cos(2\theta)\right]$$
$$+\cdots\frac{T}{2}\left[\left(1-x^{-2}\right)+\left(1-4x^{-2}+3x^{-4}\right)\cos(2\theta-\pi)\right]$$
$$(3.14\text{–}3.17)$$

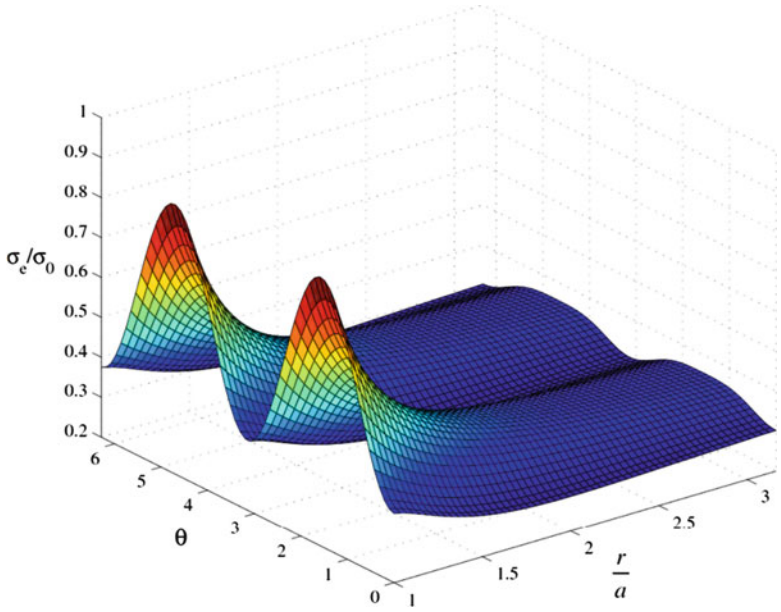

Fig. 3.7 Distribution of the microscopic effective stress in a disk-shaped unit cell containing an isotropic matrix material with a circular void with a porosity of 10 % (x = r/a, T = 0.25σ_0, L/T = 1.5). Note that the stress response is periodic with respect to theta since the matrix is isotropic (Reprinted with permission from Landry and Chen (2011). Copyright: Elsevier)

A schematic plot of the microscopic effective stress is presented in Fig. 3.7 where a very large stress concentration exists on the boundary of the void ($x = r/a = 1$). Farther away from the void, the effective stress field becomes uniform and approaches a constant value.

3.3.3 Plastic Stress State in the Unit Cell

An analytical solution exists for the fully plastic state in the case of axisymmetric loading (Kachanov 1974). In an axially symmetric loading condition, the stress components, σ_r and σ_θ become the principal stresses and the yield surface on the (σ_r, σ_θ) plane is an ellipse as shown in Fig. 3.8 for an isotropic material.

The principal stress components can be readily expressed from the parametric equations for an ellipse as

$$\sigma_r = 2\sigma_0 \cos\left(\omega + \frac{\pi}{6}\right) \tag{3.18}$$

$$\sigma_\theta = 2\sigma_0 \cos\left(\omega - \frac{\pi}{6}\right) \quad \sigma_\theta > \sigma_r \tag{3.19}$$

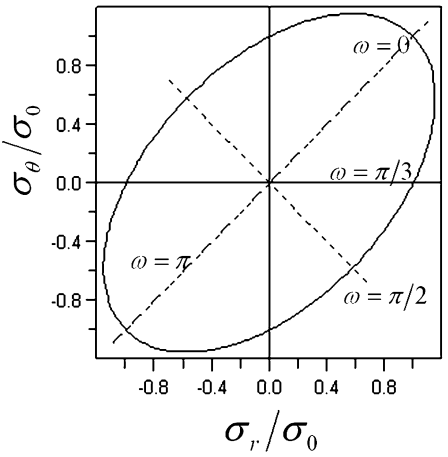

Fig. 3.8 Von Mises yield locus in the $(\sigma_r, \sigma_\theta)$ plane

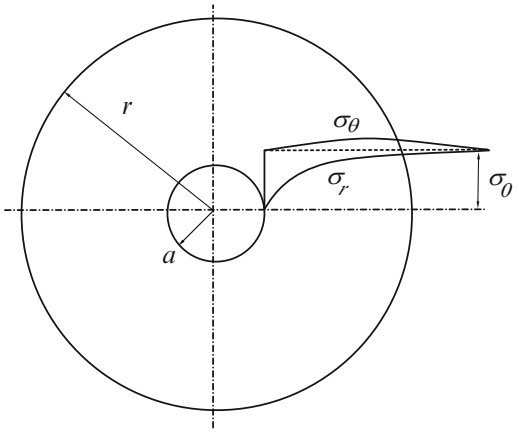

Fig. 3.9 Schematic of the stress distribution around the void in the fully plastic state under axisymmetric loading (Reprinted with permission from Xia and Chen (2007). Copyright: Springer)

where ω defines a position (stress state) on the yield locus in Fig. 3.8. For equilibrium in the radial direction

$$\frac{d\sigma_r}{dr} + \frac{\sigma_r - \sigma_\theta}{r} = 0 \tag{3.20}$$

we obtain the implicit solution to the simultaneous Eqs. (3.18), (3.19) and (3.20),

$$r^2 = \frac{C}{\sin\omega} e^{-\sqrt{3}\omega} \tag{3.21}$$

Where C is the integral constant that is determined by the boundary condition of the unit cell, i.e. $\sigma_r = 0$ on the surface of the void ($r = a$), see Fig. 3.9.

Table 3.1 Evaluation of the accuracy of the unit cell model for different unit cell sizes

Ratio (r/a)	Porosity $(a/b)^2$ (assuming $r = b$)	3.1 σ_r/σ_0 (unit-cell model)	Error percentage on σ_r/σ_0 (%)
1.5	0.444	0.360	63.98
1.7	0.346	0.452	54.81
2	0.250	0.557	44.32
5	0.040	0.894	10.57
8	0.017	0.955	4.49
10	0.010	0.971	2.94

It is straightforward to find that stress distribution decays to its uniform value in the radial direction according to

$$\left(\frac{r}{a}\right)^2 = \frac{\sqrt{3}}{2}\frac{1}{\sin\omega}e^{\sqrt{3}\left(\frac{\pi}{3}-\omega\right)} \tag{3.22}$$

A qualitative plot of the stress components σ_r and σ_θ is provided in Fig. 3.9. This method can be similarly applied to an anisotropic material through the anisotropic parameters.

A quantitative analysis of the problem shows that the distortion of the stress field distribution caused by the void tends to disappear when r/a is suffientiently large. According to the calculations in Eqs. (3.18–3.22), both σ_r and σ_θ reach σ_0 at infinity. Note that r is a measure of the distance from the void surface so that if we set a boundary in Fig. 3.6 to form an imaginary unit cell (namely set $r = b$, the outer radius of the imaginary unit cell), the porosity is $(a/b)^2$ for the planar case. However, as previously discussed, unit cell model assumes its outer boundary as the infinity. Therefore, errors are introduced in unit cell approximation with the error for various unit cell sizes presented in Table 3.1. If an error in the stress of 3 % is acceptable, the material located at a distance 10 times the void radius can be classified as being located at infinity.

3.4 Derivation of a Lower Bound Yield Criterion for Porous Sheet Metals

A lower bound solution for the isotropic matrix under a biaxial loading can be developed from the previous solutions for the microscopic stress fields in the elastic case in Eq. (3.14–3.17) since the material is elastic before the onset of yielding. As discussed in the previous section, the unit cell model creates artificial stress boundary conditions prescribed on the outer surface of the unit cell and consequently, the yield function is treated as a lower bound solution. The sheet metal matrix obeys von Mises yield criterion with the effective stress defined as

$$\sigma_{eq} = \frac{1}{\sqrt{2}}\left[\sigma_{rr}^2 + \sigma_{\theta\theta}^2 + (\sigma_{rr} - \sigma_{\theta\theta})^2 + 6\sigma_{r\theta}^2\right]^{\frac{1}{2}} \tag{3.23}$$

The matrix will begin to yield when the microscopic effective stress in a region of the cell reaches the yield limit

$$\max(\sigma_{eq}) = \sigma_0 \tag{3.24}$$

The macroscopic stresses on the outer surface of the cell are obtained by integrating over the cell volume as

$$\Sigma_{11} = \frac{1}{V}\int_V \sigma_{11} dV = (1-f)L \qquad \Sigma_{22} = \frac{1}{V}\int_V \sigma_{22} dV = (1-f)T$$
$$\Sigma_{12} = 0 \tag{3.25–3.27}$$

3.4.1 Numerical Results

Figures 3.7 and 3.10 show the distribution of the effective microscopic stress over the unit cell for two specific loading ratios (L/T). For a given loading ratio, it is straightforward to obtain the solution for the macroscopic stresses at the onset of yielding. It is worth noting that an intense stress concentration occurs on the inner surface of the unit cell that results in considerably lower yield limits due to the retention of a predominantly elastic unit cell. Therefore, the outer surface is chosen to calculate the maximum effective stress. As shown in Fig. 3.10, the onset of yielding in the unit cell is defined when the outer surface of the cell has begun to yield

$$\max\left(\sigma_e\right)\big|_{x=\sqrt{1/f}} = \sigma_0 \tag{3.28}$$

A similar technique was utilized by Gurson (1977) to account for the rigid sections in the unit cell and by Sun and Wang (1989) to construct the stress field causing a partly plastic state in the unit cell.

Figures 3.7 and 3.10 show the respective microscopic effective stresses over the entire unit cell for an entirely elastic loading scenario and an elastic–plastic loading. Note that the stresses in the elastic region of Fig. 3.10 have been scaled accordingly to generate an approximate stress surface that accommodates for load sharing between the elastic and plastic regions. The value of this scaling factor can be seen in Fig. 3.11. Approximating this value as unity imposes a maximum 5 % deviation under a void volume fraction of 0.05 for all loading paths.

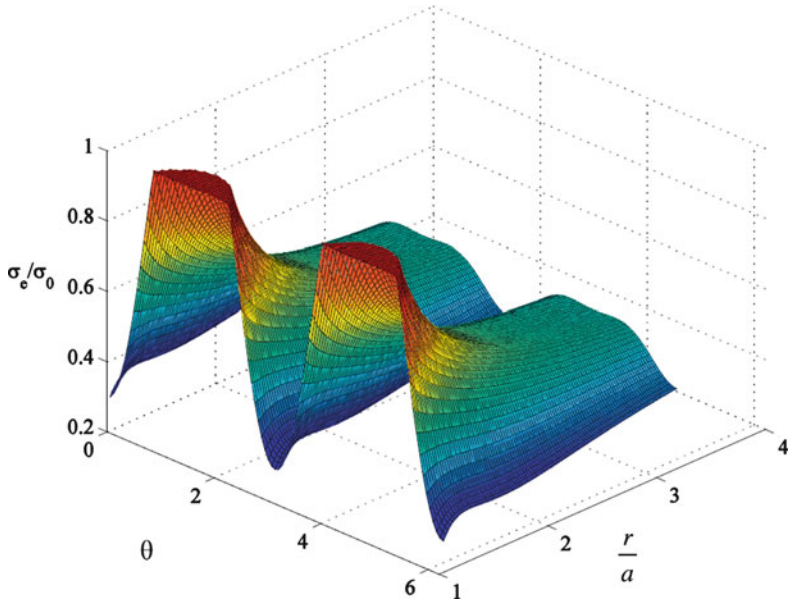

Fig. 3.10 Distribution of the microscopic effective stress in a disk-shaped unit cell containing an isotropic matrix material with a circular void with a porosity of 10 % (x = r/a, T = 0.25 σ_0, L/T = 2.0). The yield surface is truncated at unity where the material has yielded at the void surface (Reprinted with permission from Landry and Chen (2011). Copyright: Elsevier)

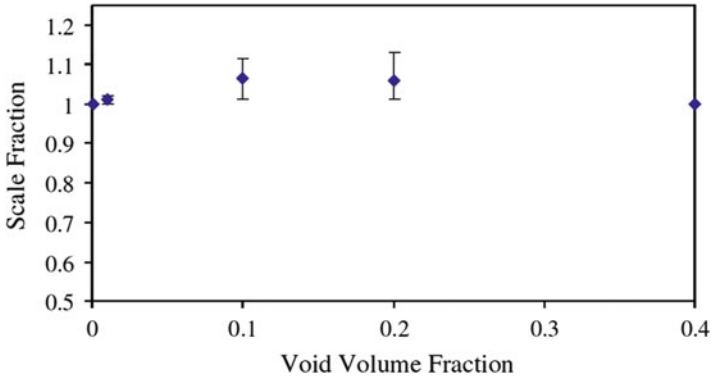

Fig. 3.11 The mean value and statistical dispersion of the load balancing scaling factor when evaluated under uniaxial, biaxial and shear loading for various void volume fractions (Reprinted with permission from Landry and Chen (2011). Copyright: Elsevier)

Following the calculation procedure discussed previously, the yield limits are numerically solved with a series of specified loading ratios (*L/T*). For simplicity, the sheet metals are assumed to have the same yield limits under tensile and compressive loadings. The numerical results are plotted with Gurson's (1977) upper bound criterion and von Mises yield function in Fig. 3.12. A comparison indicates that the

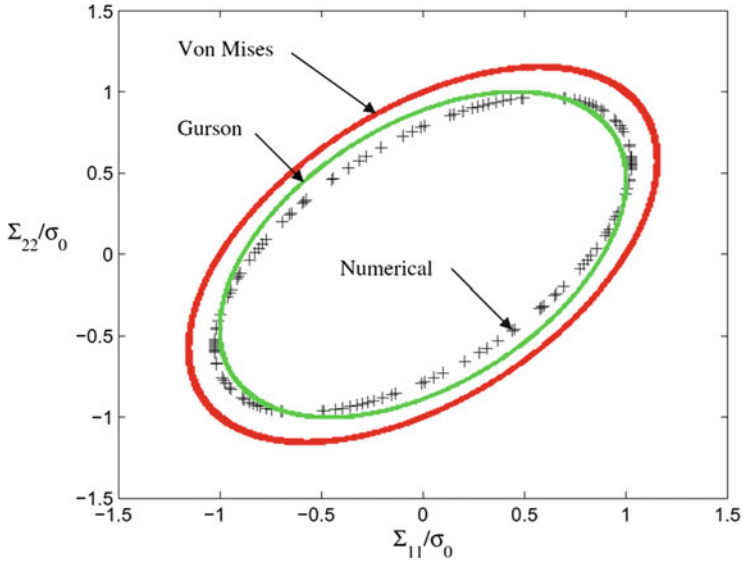

Fig. 3.12 Comparison of the numerical results for yielding in the unit cell with a porosity of 10 % compared with the yield surfaces of Gurson and von Mises (Reprinted with permission from Landry and Chen (2011). Copyright: Elsevier)

numerical results of the current model provide a more conservative yield point for uniaxial and shear loading. Due to the contrasting methodology used between the Gurson and current approach, the trend for biaxial loading shows that the Gurson yield criterion is in fact conservative in this instance. It is important to note that the yield locus never exceeds the von Mises yield locus even during equal biaxial loading due to the presence of the voids.

A closed form of the yield function is required for its practical application and this can be accomplished in a phemenological manner by introducing three fitting parameters into the equivalent stress equation in principal stress space as

$$\Phi = \Sigma_{\text{eq}} - \bar{\sigma} = 0$$

$$\Sigma_{\text{eq}} = \sqrt{1/2\left(q_1(\Sigma_{11} - \Sigma_{22})^2 + q_2\Sigma_{11}^2 + q_3\Sigma_{22}^2\right)}$$

$$q_{1-3} = \begin{cases} 8.586\, f^2 + 7.1329\, f + 1 \\ 5.857\, f^2 + 0.5734\, f + 1 \qquad f \leq 0.20 \\ 15.258\, f^2 + 2.6973\, f + 1 \end{cases} \qquad (3.29-3.31)$$

These parameters are valid for porosities up to 20 % and allows the function to revert to the von Mises yield criterion when $f = 0$. The numerical process employed here to obtain a closed form of the yield function is effective but admittedly, not mathematically elegant. The performance of Eq. (3.30) can be seen in Fig. 3.13 for a relatively large porosity of 10 %.

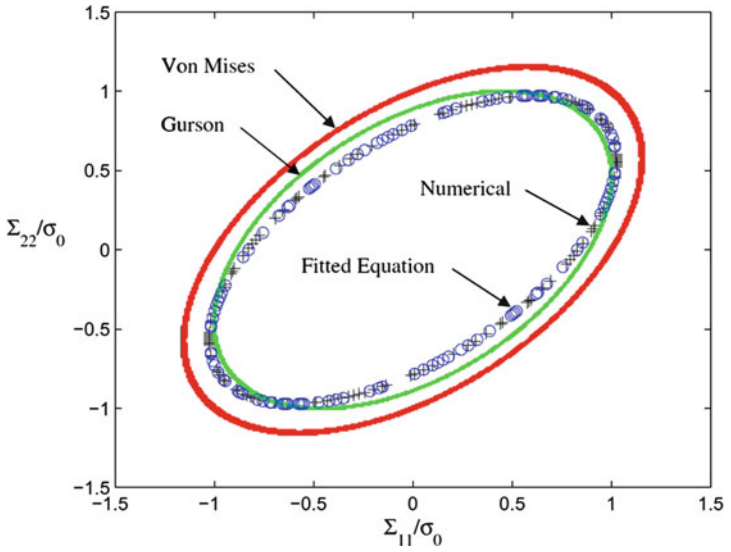

Fig. 3.13 Comparison of the numerical results for yielding in the unit cell with a porosity of 10 % compared with the fitted-yield surface in Eq. (3.25) along with the yield surfaces of Gurson and von Mises (Reprinted with permission from Landry and Chen (2011). Copyright: Elsevier)

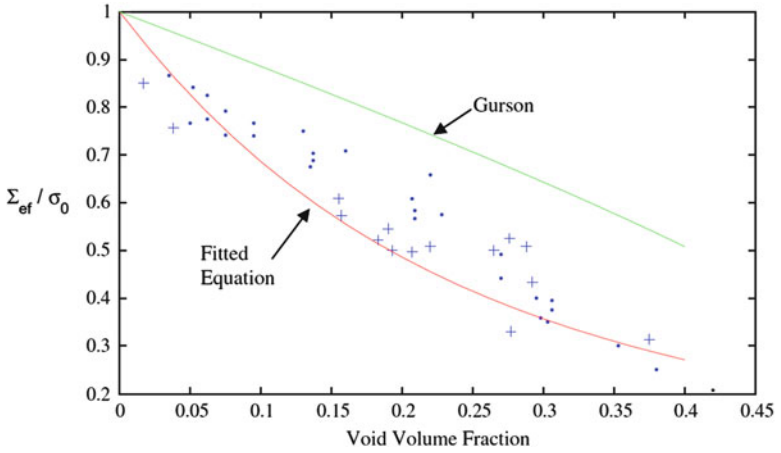

Fig. 3.14 Comparison of the fitted yield function in Eq. (3.25) and the Gurson yield criterion with the experimental results of Shima and Oyane (1976) for sintered copper specimens. The *closed dots* represent yielding in uniaxial compression while + indicates uniaxial tension (Reprinted with permission from Landry and Chen (2011). Copyright: Elsevier)

3.4.2 Comparison of the Lower Bound Solution with Experiments

The lower bound yield function in Eq. (3.29) is evaluated using the experimental results of Shima and Oyane (1976) for sintered iron and copper alloys in Figs. 3.14

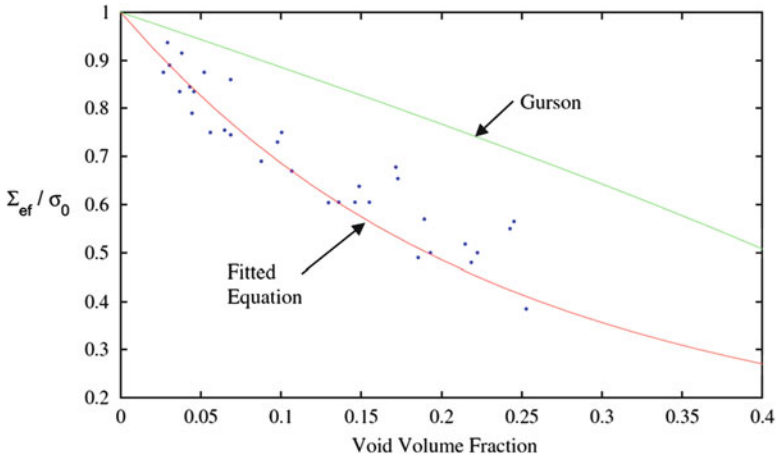

Fig. 3.15 Comparison of the fitted yield function in Eq. (3.25) and the Gurson yield criterion with the experimental results of Shima and Oyane (1976) for sintered iron specimens. The *closed dots* represent yielding in uniaxial compression (Reprinted with permission from Landry and Chen (2011). Copyright: Elsevier)

and 3.15, respectively, for a large range of porosities. For comparison, the Gurson yield surface is also evaluated. As seen previously in the work of Sun and Wang (1989), the Gurson yield criterion overestimates the yield stress and the lower bound solution performs much closer to the experimental results. For both sintered alloys, Eq. (3.29) provides a mid-range solution for lower porosities ($f < 7.5\ \%$) while its lower bound characteristics becomes apparent at higher volume fractions. It is worth noting that Shima et al.'s tests were performed for uniaxial loading and that a true evaluation of the proposed yield surface would require its application to other multi-axial stress states.

3.5 Derivation of a Quasi-Exact Lower Bound Anisotropic Yield Criterion for Porous Sheet Metals

A quasi-exact yield criterion can now be derived for anisotropic porous ductile sheet metals using the concepts and fundamentals established in the previous development of the isotropic model. The same disk-shaped unit cell is adopted under axisymmetric loading and the matrix material is assumed to be rigid-plastic and obey the Hill-48 quadratic yield function for normal anisotropy.

3.5.1 Derivation of the Flow Rule and Equivalent Plastic Strain

In cylindrical coordinates, the Hill-48 yield criterion can be written as

$$\Phi(\sigma_{ij},R)=\frac{1}{1+R}\left(\sigma_{rr}^2+\sigma_{\theta\theta}^2+R(\sigma_{rr}-\sigma_{\theta\theta})^2+2(2R+1)\sigma_{r\theta}^2\right)-\sigma_y^2=0 \quad (3.32)$$

From the associated flow rule of plasticity, the relations between the incremental plastic strain and the stress in a rigid-plastic material are

$$d\varepsilon_{rr}=d\lambda\frac{\partial F}{\partial\sigma_{rr}} \quad d\varepsilon_{\theta\theta}=d\lambda\frac{\partial F}{\partial\sigma_{\theta\theta}} \quad d\varepsilon_{r\theta}=\frac{1}{2}d\lambda\frac{\partial F}{\partial\sigma_{r\theta}}$$
$$d\lambda=\frac{1}{2}\frac{d\varepsilon_{eq}}{\sigma_{eq}} \quad (3.33-3.37)$$

Using the quadratic yield function, the stress and strain components can be expressed in matrix form using Voigt notation as

$$\begin{bmatrix} d\varepsilon_{rr}\\ d\varepsilon_{\theta\theta}\\ d\varepsilon_{zz}\\ d\varepsilon_{r\theta}\\ d\varepsilon_{rz}\\ d\varepsilon_{\theta z}\end{bmatrix}=d\lambda\left(\frac{2}{1+R}\right)\begin{bmatrix} 1+R & -R & -1 & 0 & 0 & 0\\ -R & 1+R & -1 & 0 & 0 & 0\\ -1 & -1 & 2 & 0 & 0 & 0\\ 0 & 0 & 0 & 1+2R & 0 & 0\\ 0 & 0 & 0 & 0 & 1+2R & 0\\ 0 & 0 & 0 & 0 & 0 & 1+2R\end{bmatrix}\begin{bmatrix}\sigma_{rr}\\ \sigma_{\theta\theta}\\ \sigma_{zz}\\ \sigma_{r\theta}\\ \sigma_{rz}\\ \sigma_{\theta z}\end{bmatrix} \quad (3.38)$$

that can be manipulated to obtain

$$\begin{bmatrix}\sigma_{rr}-\sigma_{\theta\theta}\\ \sigma_{\theta\theta}-\sigma_{zz}\\ \sigma_{zz}-\sigma_{rr}\\ \sigma_{r\theta}\\ \sigma_{rz}\\ \sigma_{\theta z}\end{bmatrix}=\frac{1}{d\lambda}\left(\frac{1+R}{2+4R}\right)\begin{bmatrix} d\varepsilon_{rr}-d\varepsilon_{\theta\theta}\\ d\varepsilon_{\theta\theta}-d\varepsilon_{zz}R\\ d\varepsilon_{zz}R-d\varepsilon_{rr}\\ d\varepsilon_{r\theta}\\ d\varepsilon_{rz}\\ d\varepsilon_{\theta z}\end{bmatrix} \quad (3.39)$$

By substituting Eqs. (3.39) into (3.32) the work-conjugate of the effective stress, the effective strain increment, can be expressed as

$$d\varepsilon_{\text{eq}}^2=\frac{1+R}{(1+2R)^2}\left[(d\varepsilon_{\theta\theta}-d\varepsilon_{zz}R)^2+(d\varepsilon_{zz}R-d\varepsilon_{rr})^2+R(d\varepsilon_{rr}-d\varepsilon_{\theta\theta})^2\right.$$
$$\left.+\ \frac{1+2R}{2}(d\varepsilon_{r\theta}^2+d\varepsilon_{rz}^2+d\varepsilon_{\theta z}^2)\right] \quad (3.40)$$

3.5.2 Analytical Derivation of the Yield Function

The matrix material is assumed to be ideally rigid-plastic, incompressible, and under axisymmetric loading, i.e.

$$\Sigma_{rr} = \Sigma_{\theta\theta} = L \quad \Sigma_{zz} = T \quad \Sigma_{r\theta} = \Sigma_{z\theta} = \Sigma_{zr} = 0 \tag{3.41a–c}$$

where Σ_{ij} are the macroscopic stress components; L is the macroscopic stress in the sheet plane, and T is the macroscopic stress normal to the sheet plane. In axisymmetric loading with planar isotropy and normal isotropy, the microscopic strain rate in the z-direction, the thickness direction of the sheet, that is normal to the unit-cell plane is

$$d\varepsilon_z = dE_z \tag{3.42}$$

where dE_z is the macroscopic strain increment that is assumed to be independent of the radius, r. The boundary conditions associated with the unit-cell model are

$$\sigma_{rr}|_{r=a} = 0 \quad \sigma_{rr}|_{r=b} = L \tag{3.43a, b}$$

The shear stresses, shear strains and the circumferenctial velocity are all zero for axisymmetric loading

$$\sigma_{r\theta} = \sigma_{rz} = \sigma_{z\theta} = 0 \quad d\varepsilon_{r\theta} = d\varepsilon_{rz} = d\varepsilon_{z\theta} = 0 \quad v_\theta = 0 \tag{3.44a–c}$$

and the equilibrium equation in the radial direction becomes

$$\frac{\partial \sigma_{rr}}{\partial r} + \frac{1}{r}(\sigma_{rr} - \sigma_{\theta\theta}) = 0 \tag{3.45}$$

with incremental strains defined as

$$d\varepsilon_{rr} = \frac{\partial v_r}{\partial r} \quad d\varepsilon_{\theta\theta} = \frac{v_r}{r} \tag{3.46a, b}$$

The assumption of a rigid incompressible matrix material leads to the volume conservation constraint

$$d\varepsilon_{rr} + d\varepsilon_{\theta\theta} + d\varepsilon_{zz} = 0 \tag{3.47}$$

Combining equations (3.42), (3.46) and (3.47), the radial velocity is

$$v_r = \frac{A}{r} - \frac{r}{2} dE_z \tag{3.48}$$

where A is an integration constant that is independent of r and related to the anisotropic parameter, R, and the void volume fraction, f. Substituting the radial velocity (3.48) into (3.46), we obtain

$$d\varepsilon_{rr} = -\frac{A}{r^2} - \frac{1}{2}dE_z \quad d\varepsilon_{\theta\theta} = \frac{A}{r^2} - \frac{1}{2}dE_z \tag{3.49a, b}$$

The effective strain rate is obtained by substituting Eqs. (3.42) and (3.49) into (3.40)

$$d\varepsilon_{eq}^2 = \frac{1+R}{(1+2R)}\left[\frac{2A^2}{r^4} + \left(\frac{1}{2}+R\right)dE_z^2\right] \tag{3.50}$$

3.5.3 Solution for the Macroscopic Radial Stress

According to the flow rule, and because $\sigma_{\text{eq}} = \sigma_0$ in the completely plastic state

$$\sigma_{rr} - \sigma_{\theta\theta} = -\sqrt{\frac{1+R}{1+2R}}\frac{2\sigma_0 A/r^2}{\sqrt{\left[\frac{2A^2}{r^4} + \left(\frac{1}{2}+R\right)dE_z^2\right]}} \tag{3.51}$$

Using (3.51) in the equilibrium Eq. (3.45) results in

$$\begin{aligned}\sigma_{rr} &= -\int_a^r \frac{\sigma_{rr} - \sigma_{\theta\theta}}{r}dr \\ &= -\sigma_0\sqrt{\frac{1+R}{1+2R}}\int_a^r \frac{\sqrt{2}(\sqrt{2}A/r^2)}{\sqrt{\left[\left(\frac{\sqrt{2}A}{r^2}\right)^2 + \left(\frac{1}{2}+R\right)dE_z^2\right]}}\frac{1}{r}dr\end{aligned} \tag{3.52}$$

Define new variables as

$$c = dE_z\sqrt{\left(\frac{1}{2}+R\right)} \quad x = \frac{\sqrt{2}A}{cr^2} \quad B = \sqrt{\frac{1+R}{1+2R}} \tag{3.53a–c}$$

Manipulating the identity in Eq. (3.53b), we obtain

$$\frac{1}{r}dr = -\frac{1}{2x}dx \tag{3.54}$$

Using Eqs. (3.53) and (3.54) in (3.52), σ_{rr} is solved as

$$\sigma_{rr} = \frac{\sqrt{2}}{2}\sigma_0 B\left[\sinh^{-1}x_a - \sinh^{-1}x\right] \tag{3.55}$$

where $x_a = \frac{\sqrt{2}A}{ca^2}$. Similarly, we define $x_b = \frac{\sqrt{2}A}{cb^2}$. According to the boundary condition (3.41), the boundary radial stress is

$$\Sigma_{rr} = \sigma_{rr}|_{r=b} = L = \frac{\sqrt{2}}{2}\sigma_0 B\left[\sinh^{-1}x_a - \sinh^{-1}x_b\right] \tag{3.56}$$

3.5.4 Solution for the Macroscopic Through-Thickness Stress

By definition, the macroscopic stress Σ_{zz} is

$$\Sigma_{zz} = \frac{2}{b^2}\int_a^b \sigma_{zz} r dr \tag{3.57}$$

The normal stress is manipulated as

$$\sigma_{zz} = \sigma_{rr} + (\sigma_{zz} - \sigma_{rr}) \tag{3.58}$$

Substituting Eqs. (3.42), (3.49) and (3.50) into (3.53c) gives

$$\sigma_{zz} - \sigma_{rr} = \frac{1+R}{1+2R}\frac{\sigma_0}{d\varepsilon_{eq}}(d\varepsilon_{zz}R - \dot{\varepsilon}_{rr}) = \sigma_0 B\frac{\sqrt{2}x/2 + m}{\sqrt{x^2+1}}$$
$$m = \sqrt{\frac{1}{2}+R} \tag{3.58a, b}$$

Substituting Eqs. (3.55), (3.58) into (3.57) results in

$$\Sigma_{zz} = T = -B\sigma_0 x_b\left\{\frac{\sqrt{2}}{2}\left(\sinh^{-1}x_a\right)\int_{x_a}^{x_b} x^{-2}dx - \frac{\sqrt{2}}{2}\int_{x_a}^{x_b} x^{-2}\left(\sinh^{-1}x\right)dx + \frac{\sqrt{2}}{2}\int_{x_a}^{x_b}\frac{1}{x\sqrt{x^2+1}}dx + m\int_{x_a}^{x_b}\frac{1}{x^2\sqrt{x^2+1}}dx\right\}$$

Note the second term is

$$\frac{\sqrt{2}}{2}\int_{x_a}^{x_b} x^{-2}\left(\sinh^{-1}x\right)dx = -\frac{\sqrt{2}}{2}\left[\frac{1}{x}\sinh^{-1}x\right]_{x_a}^{x_b} + \frac{\sqrt{2}}{2}\int_{x_a}^{x_b}\frac{1}{x\sqrt{x^2+1}}dx$$

Therefore,

$$T = L + \sigma_0 B x_b m \left[\sqrt{\frac{1}{{x_a}^2} + 1} - \sqrt{\frac{1}{{x_b}^2} + 1} \right] \tag{3.59}$$

3.5.5 *Solution for the Yield Function*

Noting that $f = x_b/x_a$, Eq. (3.59) can be rewritten as

$$\left(\frac{T-L}{\sigma_0} \right)^2 = \frac{1+R}{2} \left[1 + f^2 - 2f \left(\sqrt{(1+{x_b}^2)(1+{x_a}^2)} - x_a x_b \right) \right] \tag{3.60}$$

Rearranging Eq. (3.56), we can obtain

$$\frac{\sqrt{2}L}{\sigma_0 B} = \frac{\sqrt{2}L}{\sigma_0} \sqrt{\frac{1+2R}{1+R}} = \left(\sinh^{-1} x_a - \sinh^{-1} x_b \right) \tag{3.61}$$

Using the following identity

$$\cosh\left(\sinh^{-1} x_a - \sinh^{-1} x_b \right) = \sqrt{(1+{x_b}^2)(1+{x_a}^2)} - x_a x_b \tag{3.62}$$

and combining Eqs. (3.60), (3.61) and (3.62) give

$$\left(\frac{T-L}{\sigma_0} \right)^2 = \frac{1+R}{2} \left[1 + f^2 - 2f \cosh \left(\sqrt{\frac{1+2R}{1+R}} \frac{\sqrt{2}L}{\sigma_0} \right) \right] \tag{3.63}$$

The macroscopic effective stress in the Hill-48 yield criterion is

$$\Sigma_{\text{eq}}^2 = \frac{1}{1+R} \times \left[(\Sigma_{22} - \Sigma_{33})^2 + (\Sigma_{33} - \Sigma_{11})^2 + R(\Sigma_{11} - \Sigma_{22})^2 + 2(1+2R)\Sigma_{12} \right] \tag{3.64}$$

Note $L = \frac{1}{2}(\Sigma_{11} + \Sigma_{22})$ and $\Sigma_{\text{eq}}^2 = \frac{2}{1+R}(T-L)^2$ thus, an equivalent form of Eq. (3.63) is obtained. Finally, the yield function is expressed as (Xia and Chen 2007)

$$\left(\frac{\Sigma_{\text{eq}}}{\sigma_0} \right)^2 + 2f \cosh \left(\sqrt{\frac{1+2R}{2(1+R)}} \frac{3\Sigma_{\text{hyd}}}{\sigma_0} \right) - 1 - f^2 = 0 \tag{3.65}$$

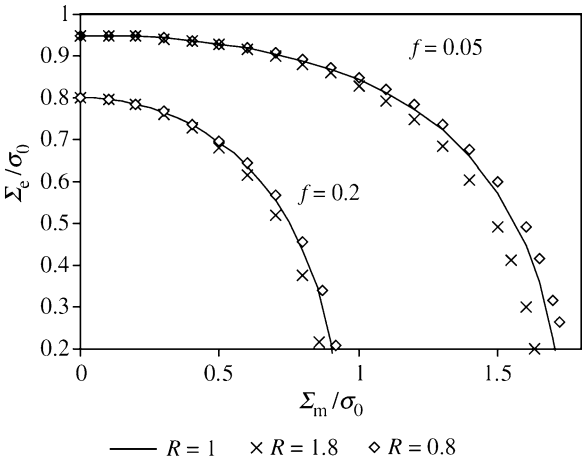

Fig. 3.16 Comparison of the yield loci of the current yield function (3.61) for various values of R and f. The *solid curves* indicate the yield loci for isotropic materials (R = 1) (Reprinted with permission from Xia and Chen (2007). Copyright: Springer)

When $R = 1$, the yield function (3.65) is reduced to the derivation of Gurson (1977) for a cylindrical unit cell subjected to axisymmetric loading

$$\left(\frac{\Sigma_{eq}}{\sigma_0}\right)^2 + 2f\cosh\left(\sqrt{3}\frac{3}{2}\frac{\Sigma_{hyd}}{\sigma_0}\right) - 1 - f^2 = 0 \tag{3.66}$$

3.5.6 *Effect of Mechanical Anisotropy in a Porous Ductile Material*

Two different R values, 0.8 and 1.8, are selected to quantify the influence of mechanical anisotropy on the yield surface in Fig. 3.16 for FCC and BCC materials, respectively. The material does not possess any void-induced anisotropy since the void is assumed to remain circular during deformation. The yield surface contracts slightly with an increase in the R-value for a constant porosity, indicating that anisotropy increases pressure sensitivity. The effect of anisotropy becomes more pronounced in plane stress loading as demonstrated in Fig. 3.17.

It is worth noting that for a given porosity value, the yield points on the vertical axis for various R values (Fig. 3.17) coincide with each other. This implies that for pure shear, the yield behavior of porous sheet metal is independent of normal anisotropy. It should be cautioned however that the influence of shear may be different if a cubic unit cell geometry was assumed. The cylindrical unit cell geometry is restricted to axisymmetric stress states resulting in a yield criterion that is independent of the third invariant of the stress deviator that is used to characterize shear loading via the lode parameter. The variational model of Danas and Ponte Casteneda (2009) shows evidence of the third stress invariant on

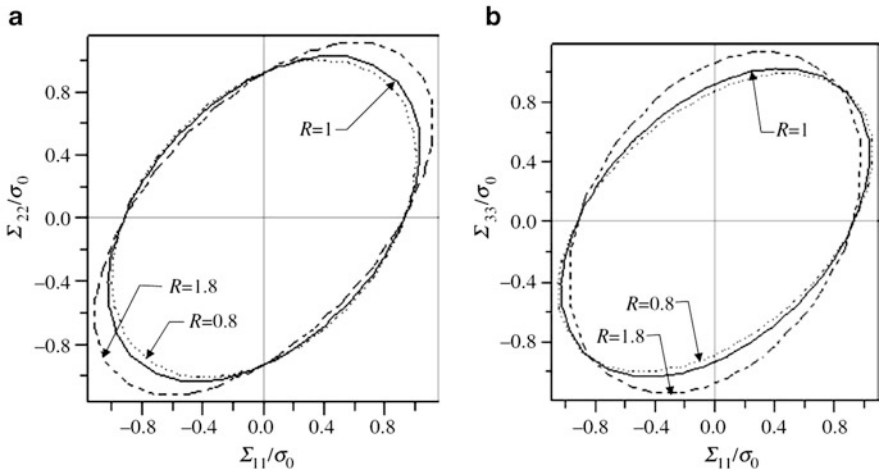

Fig. 3.17 Yield loci for various R values for a porosity of 5 % in the (**a**) Σ11–Σ22 plane and (**b**) Σ11–Σ33 plane (Reprinted with permission from Xia and Chen (2007). Copyright: Springer)

yielding of a porous ductile material. As expected, the influence of the R-value becomes more pronounced at higher stress triaxialities since the R-value acts as a scaling factor for the hydrostatic stress dependence of the yield surface.

3.5.7 Assessment of the Uniqueness of the Current Yield Function

A limitation of the unit-cell model is that the geometry of the unit-cell must be constructed so that the specified porosity is satisified even though the cell may not be large enough for the outer surface to be regarded as infinity (Gurson 1977). In this sense, the stress field inside the unit cell could be considered a statically admissible stress field and the yield function in Eq. (3.65) would be classified as an analytical lower bound solution rather than an exact solution. If one takes this view, the current yield function can provide a benchmark to assess other lower bound yield criteria. Conversely, if we ignore the limitation of the unit cell model, the only remaining approximation is that the normal strain rate is independent of the unit cell radius. This limitation can be reasonably ignored for a comparison between unit cell models and since the unit cell is assumed to be in a fully plastic state, the yield stress is likely overestimated since the actual unit cell would likely contain rigid regions. From this perspective, the current solution could be interpreted as an analytical solution and used to evaluate upper bound yield criteria. In other words, the uniqueness of the current model may make it a valuable reference for a variety of situations.

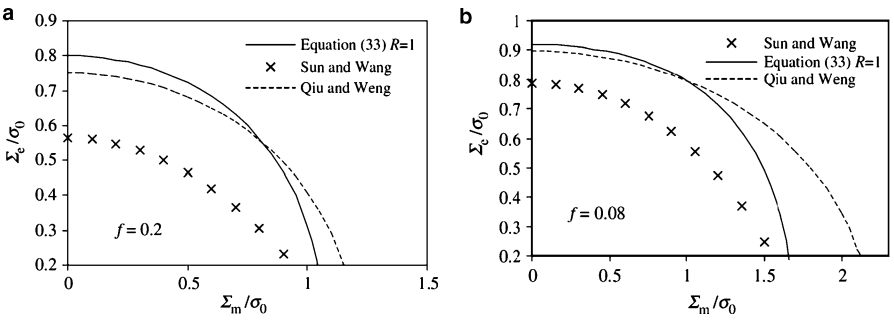

Fig. 3.18 Comparison between the current yield function (3.64) with Sun and Wang's lower bound yield function (Eq. 2.31), and Qiu and Weng's energy based yield function, Eq. (2.31) (Reprinted with permission from Xia and Chen (2007). Copyright: Springer)

As an example, the lower bound solution of Sun and Wang (1989) and the energy-based solution of Qiu and Weng (1993) are compared with the current yield function. In Sun and Wang's derivation, the stress field in a spherical unit-cell was decomposed into an elastic and plastic part. Qiu and Weng (1993) eschewed the unit cell approach and derived a yield criterion for randomly- oriented voids using an energy-based approach to obtain

$$\left(\frac{\Sigma_{eq}}{\sigma_0}\right)^2 + \frac{f}{4\left(1+\frac{2}{3}f\right)}\left(3\frac{\Sigma_{hyd}}{\sigma_0}\right)^2 - \frac{(1-f)^2}{1+\frac{2}{3}f} = 0 \tag{3.67}$$

It is worth noting that the Sun and Wang and Qiu and Weng models were derived for spherical voids while the current yield function assumes circular (cylindrical) voids. To provide an equal comparison, a scale factor of $1/\sqrt{3}$ is applied to the the hydrostatic stress component in Eq. (3.65) with reference to the Gurson's (1977) conversion from the cylindrical model to the spherical void yield criterion as

$$\left(\frac{\Sigma_{eq}}{\sigma_0}\right)^2 + 2f\cosh\left(\sqrt{\frac{1+2R}{6(1+R)}}\frac{3\Sigma_{hyd}}{\sigma_0}\right) - 1 - f^2 = 0 \tag{3.68}$$

It is more reasonable to compare yield function (3.68) with Sun and Wang's yield function (Eq. 2.31) and Qiu and Weng's yield function (3.67).

Figure 3.18 shows the yield loci of Eq. (3.22) with $R = 1$ in comparison with Sun and Wang's (1989) lower bound yield function (Eq. 2.31) and Qiu and Weng's (1993) yield function in Eq. (3.67). Large discrepancies are observed between the current yield function and Sun and Wang's criterion, as shown in both figures. This is because the unit cell in Sun and Wang's lower bound approach is assumed to be partially plastic while the cell was assumed to be completely plastic in our derivation. In contrast, the current yield loci are in better agreement with Qiu and Weng's results who considered both the elastic and plastic energies in the material.

3.5.8 *Evaluation of the Quasi-Exact Anisotropic Yield Criterion*

If the prescribed stresses and normal strain rate are assumed to be actual quantities, the yield criterion should be considered an "exact" solution because the macroscopic stresses in the unit cell were direcly obtained from the equilibrium equation. However, it is better to describe the yield function as "quasi-exact" due to the assumed independence of the normal strain rate on the unit cell radius. The other principal source of error in the model can be attributed to the prescribed boundary condition on the unit cell that can lead to significant errors for high porosities as discussed in Sect. 3.3.3. Fortunately, this model has been developed for application to sheet materials where the porosities at failure are on the order of a few percent.

It is important to discuss the work of Liao et al. (1997) who obtained the same result as Eq. (3.65) using the upper bound theory of plasticity by decomposing the velocity field into volume and shape-changing fields and then constructing each field seperately. Although the resulting yield surfaces are equivalent, very different mathematical approaches were used to obtain the macroscopic yield stress. Consequently, the model of Liao et al. (1997) is approximate since Eq. (3.65) was derived from the analytical stress field solutions in the unit cell. From the perspective of extremum theory, the model of Liao et al. (1997) is an upper-bound solution whilst Eq. (3.65) is an "exact" solution.

The current result coincides with the yield surface of Liao et al. (1997) for the following reasons:

- The same disk-shaped unit cell geometry was used and subjected to axisymmetric loading
- Similar form of solutions to the velocity fields: Liao et al. (1997) utilized the flow rule and the equilibrium equation while the present method solves for the velocity fields directly from volume conservation.
- Both models assume that the matrix material in the unit cell has achieved a completely plastic state

It is also interesting to note that the anisotropic yield function of Benzerga and Besson (2001) for porous orthotropic materials also reduces to Eq. (3.68) when simplified to normal anisotropy. In the model of Benzerga and Besson (2001), the velocity field was envisaged as a linear combination of Rice and Tracey's (1969) solution for volume change and the other is for a uniform shape change. Strictly speaking, the present result should not be considered to be a special case of Benzerga and Besson (2001) since their result is also an approximate upper bound solution like the model of Liao et al. (1997).

Despite that the closed form yield function is derived under an axisymmetric loading condition, it still remains valid and provides acceptable predictions of plastic deformation under universal loading conditions as investigated by Liao et al. (1997) for rigid plastic materials, and Chien et al. (2001) for a three-dimensional unit cell of hardening materials. Liao et al. generated all possible planar deformation modes by specifying the macroscopic strain rate ratio

dE_{11}/dE_{22} and obtained the corresponding solutions for the macroscopic stresses Σ_{11} and Σ_{22}. Their numerical results indicate that the closed form yield criterion matches well with the numerical results. Also, as Benzerga and Besson (2001) discussed about Gurson's results (1977) although Gurson considered axisymmetric loading conditions, it was proved by Leblond et al. (1995) that the analysis and corresponding results remain valid for general loading conditions.